IET Generation, Transmission & Distribution

Research Article

IET Journals
The Institution of Engineering and Technology

S-shaped droop control method with secondary frequency characteristics for inverters in microgrid

ISSN 1751-8687
Received on 2nd May 2016
Accepted on 1st June 2016
doi: 10.1049/iet-gtd.2016.0673
www.ietdl.org

Jun Li[1,2], Fangxing Li[2] ✉, Xianyun Li[1], Haitao Liu[1], Fan Chen[1], Bailiang Liu[3]

[1]*School of Electric Power Engineering, Nanjing Institute of Technology, Nanjing, People's Republic of China*
[2]*Department of EECS, The University of Tennessee, Knoxville, TN, 37996, USA*
[3]*State Grid Jiangsu Electric Power Company Economic Research Institute, Nanjing, People's Republic of China*
✉ *E-mail: fli6@utk.edu*

Abstract: Microgrid technologies have been studied for various goals including enabling renewable energy penetration. Traditional droop control is important for microgrids to achieve plug and play characteristics, but it may not be suitable for storage units with time-varying capacity levels due to the constant slope in droop control. In order to address the potential challenges of dynamic adjustment in linear droop control applied to microgrid inverters powered by limited energy sources, this study presents an S-shaped droop control. This control method tends to make the inverter to output more power when the frequency is close to the nominal operating point, while outputting less power when the frequency is away from the nominal operating point such that the other generators will pick up more load. Also, power quality problems can be addressed with the improvement provided by the characteristic similar to the secondary frequency control which brings the frequency closer to the rated frequency. The proposed mathematical model is built by curve fitting and theoretic analysis, and is simulated in Matlab/Simulink. The results verified the ability to improve power quality and adjust the load share among inverters as opposed to conventional droop control.

Nomenclatures

f	generation output frequency
P	generation output active power
f_0	generation output frequency when no load demand
f_N	generation output frequency when rated load power demand
$f_{\min}$	generation minimum output frequency allowed
P_N	generation output active power when rated load power demand
$P_{\max}$	generation maximum output active power
$P_{LA(1)} \cdots P_{LA(n)}$	n load-frequency curves between the intersection point A and point N in Fig. 1
$P_{LB(1)} \cdots P_{LB(m)}$	m load-frequency curves between the intersection point B and point N in Fig. 1
U, $U_{\min}$ and $U_{\max}$	generation output voltage, minimum limit, and maximum limit
Q, $Q_{\min}$ and $Q_{\max}$	generation output reactive power, minimum limit, and maximum limit
Δf	frequency variation
ΔP	active power variation
ΔU	voltage magnitude variation
ΔQ	reactive power variation
$\mathrm{d}f/\mathrm{d}P$	speed ratio of output active power against frequency
$\mathrm{d}U/\mathrm{d}Q$	speed ratio of output reactive power against voltage
k_f	$\mathrm{d}f/\mathrm{d}P$ value in linear droop control
k'_f	$\mathrm{d}f/\mathrm{d}P$ value in S-shaped droop control
k_u	$\mathrm{d}U/\mathrm{d}Q$ value in linear droop control
k'_u	$\mathrm{d}U/\mathrm{d}Q$ value in S-shaped droop control
k_{f0}	$\mathrm{d}f/\mathrm{d}P$ value, when no load demand, in linear droop control in Fig. 2
k'_{f0}	$\mathrm{d}f/\mathrm{d}P$ value, when no load demand, in S-shaped droop control in Fig. 2
k'_{fi0}	different $\mathrm{d}f/\mathrm{d}P$ values, when no load demand, corresponding to different droop curves in Fig. 3
k_{u0}	$\mathrm{d}U/\mathrm{d}Q$ value, when no load demand, in linear droop control in Fig. 2
k'_{u0}	$\mathrm{d}U/\mathrm{d}Q$ value, when no load demand, in S-shaped droop control in Fig. 2
a_f, b_f, c_f, and d_f	polynomial coefficients in (1)
P_{L0}	load power
ΔP_{L0}	load change quantity
f_s	frequency in S-shaped control
Δf_s	frequency variation in S-shaped control
K_L	static frequency adjustment effect coefficient of load
ΔP_{2s}	output power variation of the second source by S-shaped droop control
ΔP_2	output power variation of the second source by linear droop control
k_{fi}	$\mathrm{d}f/\mathrm{d}P$ value of source i by linear droop control in (3) and (4)
k'_{fi}	$\mathrm{d}f/\mathrm{d}P$ value of source i by S-shaped droop control in (3) and (4)
a_u, b_u, and c_u	polynomial coefficients in (8)

1 Introduction

Microgrids play an important role in smart distribution networks via a flexible transition between the grid-connected and the islanded modes. The peer-to-peer control [1–8] strategy provides the inherent advantage of seamless mode switching in microgrids. By now, the aim of the above strategy is usually obtained by linear droop control technique for inverters, which can be consistently applied in either the grid connected mode or the islanded mode [9, 10]. One of the challenges of the primary droop frequency control strategy is the deviation from the normal frequency/voltage

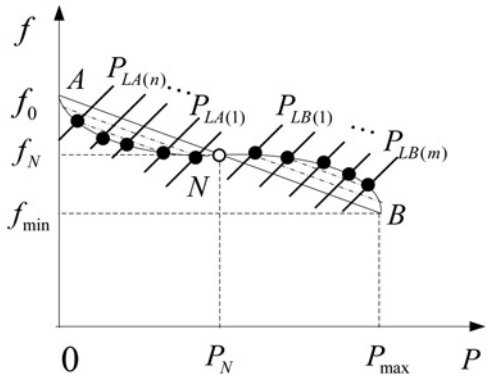

Fig. 1 *Generator secondary frequency operating points trajectory schematic*

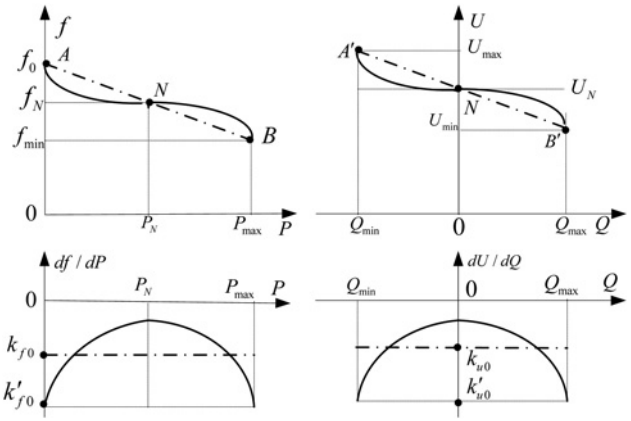

Fig. 2 *S-shaped droop curve and ratio curve*

magnitude under a large load variation which may result in power quality problems. The method of adding an integral action to the droop controller improves the frequency deviation as discussed in the previous works [4, 11], but this is not suitable in the islanded mode. The authors in [12, 13] improve the above method in the islanded mode by increasing the number of integral loops, however, more integral loops may weaken the response speed of the controller. A distributed hierarchical structure is presented in [14, 15] with common communication in the islanded microgrid to improve the frequency deviation. Since the above method depends on the communication, a fault in communication may impact the islanded operation. Therefore, the motivation of this research work is to investigate a possible method to improve the frequency control based on the proportional element.

Meanwhile, the linear droop control cannot be applied directly in the storage units due to their limited energy supply. The storage units are important for maintaining stable operation in the islanded microgrid. According to the storage unit power output variation, a novel droop control strategy is needed to adjust the output with load variation and the varying capacity of the storage unit.

With the above motivation, a new control method, called S-shaped droop control, is proposed in this paper to address the challenge of large deviation that arises due to linear droop control in microgrid inverters. In the proposed control, the droop coefficients are adjusted according to the current load demand, and the output power can be altered. As a result, the secondary control characteristics for adjusting the frequency will be naturally included in the proposed droop control and provide better results. The secondary control characteristics can also be applied to voltage amplitude regulation for improved effect. Meanwhile, the method can change the output power of an inverter source with limited energy supply (such as energy storage units) according to practical operation conditions. Thus, it can be applied to the control of these sources.

The remaining part of this paper is organised as follows. The primary droop and secondary droop characteristics in a synchronous generator is described in Section 2, which analyses the improvement of secondary frequency regulation and the feasibility in inverter control. Section 3 introduces microgrid inverter droop control with secondary frequency control characteristics and the S-shaped droop concept. In this section, the theoretic comparison between traditional linear droop and the proposed S-shaped droop is carried out. The design principles and the mathematical models are discussed. Sections 4 and 5 analyse the S-shaped droop with P–f and Q–U controls, respectively, among multi-inverters. Section 6 presents the method of implementing the S-shaped droop characteristic in inverter control. In Section 7, the simulation study of a test system consisting of two inverter-based sources between the proposed droop case and the contrast case is implemented, and the active power, reactive power and frequency dynamics are analysed. In Section 8, conclusions are provided.

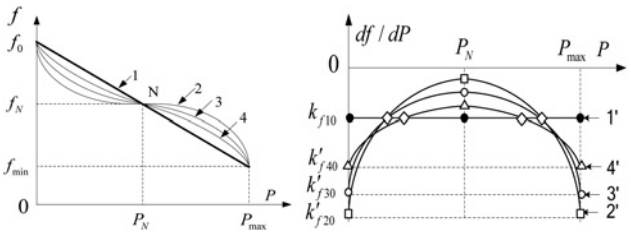

Fig. 3 *S-shaped P–f droop curve and df/dP ratio curve design*

2 Primary droop and secondary droop characteristics in synchronous generator

The usual droop control characteristics in inverters are originally borrowed from the power output characteristics of the synchronous generator [7]. Although a load increment outside of the regular range results in a large deviation of frequency or a lower power quality, a secondary adjustment can be used to achieve better frequency regulation.

The secondary control command for adjusting the frequency is issued by the control centre and then the operation is implemented via a manual or automatic operation of a speed-changer service motor to change the load reference set point. This will cause the frequency characteristics to move in parallel (a shift up represents an output power increase and a shift down represents an output power decrease) such that the frequency deviation caused by a large load change can be kept within the allowable range. By doing so, the system's performance in frequency regulation will be improved.

Taking the load increase as an example, the secondary frequency control effect causes the power curve to shift upward via a change of intake air or intake water to the prime mover such that the frequency deviation decreases and the load demand is met. In Fig. 1, the dash-and-dot lines parallel with the linear droop curve AB represent the consequence of the secondary frequency adjustment, and the intersection points between points N and B, namely m intersection points between m load–frequency curves ($P_{LB(1)} \cdots P_{LB(m)}$) and the generator power output curves in parallel, represent a different operation points with load increasing. The intersection points of the decreasing load-frequency curves ($P_{LA(1)} \cdots P_{LA(n)}$) and the generator power output curves between N and A points follow a similar interpretation. The movement trajectory of the above intersection locations shows an S-shaped curve, which can be used in the droop control of the inverter with the effect of secondary frequency regulation.

3 Microgrid inverter droop control with secondary frequency control characteristics

3.1 Concept of S-shaped droop curve

The conventional droop characteristics in inverter sources are linear, which means that the slope coefficient is constant in the range between its maximum and minimum output. In other words, microsources utilising this linear droop control strategies keep the ratio of frequency variation versus active power variation, i.e. $\Delta f/\Delta P$, constant regardless of whether the size or capacity of the output power approaches the output limit. Similar approaches are applied to voltage regulation droop control considering voltage magnitude variation ΔU and reactive power variation ΔQ. The linear droop curve and the ratio are denoted by dotted line as shown in Fig. 2.

In Fig. 2, the abscissa scale in the upper P–f curve and lower curve of $\mathrm{d}f/\mathrm{d}P$ against P (or the upper Q–U curve and the lower curve of $\mathrm{d}U/\mathrm{d}Q$ against Q for Q–U control) are identical. In the figure, P and Q denote the microsource active and reactive output powers, respectively; f_0 is the frequency with no load; f_N is the nominal frequency; $f_{\min}$ is the allowed minimum frequency; U_N is the nominal voltage with zero reactive power output; $U_{\max}$ and $U_{\min}$ denote the maximum and minimum voltages, respectively; k_f and k_u are negative constants that denote slope coefficients in linear P–f and Q–U droop curves, respectively.

The speed ratio of output power (k_f in Fig. 2) is constant in linear droop control which does not match the desired power output dynamics of the inverter-based microsource with limited energy capacity. The expected dynamics for the inverter output include two aspects:

- First, if the operating point is near the nominal operation point with rated frequency and voltage, load fluctuations should be met as soon as possible with the frequency fluctuation being as small as possible.
- Second, when the output power is close to the upper or lower limit of the microsource capacity, the share of total load to this microsource should be smaller than the share to other sources since it has less room to vary its output.

To realise the above two goals, a modification of the linear droop curve is necessary and the power output needs to be regulated at variable rates based on the operating condition. To retain the inherent advantages of automatic load sharing and synchronisation, the droop characteristics should be kept in the proposed new control strategy. However, the shape of the droop curve may be modified to the S-shaped droop curve, denoted by a solid line as shown in Fig. 2.

While the droop characteristic is preserved, the speed ratio of ΔP against Δf (resp. ΔQ against ΔU) is no longer constant. The above speed ratios can change with the current operation characteristics, such as the present output power and the amounts of energy in the storage units. For example, in the case of the S-shaped curve in the P–f plane, the absolute value of $\mathrm{d}f/\mathrm{d}P$ can reflect the speed ratio change in the P–f curve. If the vicinity of the nominal point $\mathrm{d}f/\mathrm{d}P$ is close to zero, i.e. the absolute value of $\Delta P/\Delta f$ is very large, the output power speed ratio of the inverter is at its maximum with very high sensitivity to load fluctuations. Thus, the output power can quickly compensate for power imbalance as less frequency deviation as possible. This design matches the practical operation of the inverter (i.e. when the microsource is operating near the nominal point, the efficiency reaches its maximum) such that the desired power output can be quickly achieved. On the other hand, with power output close to the power limit (0 or $P_{\max}$), the $\mathrm{d}f/\mathrm{d}P$ absolute value reaches its maximum. This means that a small load change can cause a relatively large frequency fluctuation. With the limited capacity of energy storage, the inverter will adjust the present output power according to the amount of load demand and the duration requirements of power supply to obtain the optimal operation. Therefore, the load share percentage for the inverter close to the limits of energy output capacity will be smaller than the percentage for the other inverters in normal operation.

3.2 S-shaped curve design

The design of the S-shaped droop curve can be obtained via adjustment of the linear droop curve. With the S-shaped P–f droop curve design as an example shown in Fig. 3, the droop curve design must meet the existing output power limits (0 and $P_{\max}$) while also meeting the P_N and f_N values corresponding to the nominal operating point N in Fig. 3. The above requirements should not change the physical characteristics of the power source on the DC side. The S-shaped P–f droop curve design is schematically shown in Fig. 3.

In Fig. 3, curve 1 is a linear droop curve with 2, 3, and 4 denoting different S-shaped droop curves. As seen in Fig. 3, curves 2, 3, and 4 all satisfy the output power boundaries and the nominal point requirements.

The key to the proposed S-shaped droop curve design is the $\mathrm{d}f/\mathrm{d}P$ value setting at the nominal point, i.e. point N in Fig. 3. The $\mathrm{d}f/\mathrm{d}P$ value determines the slope at the point N on the P–f curve, which further determines the slope tendency of the curve in sections other than the N point. In Fig. 3, the absolute values of the slope at N in curves 2, 3, and 4 gradually increase, thus three different S-shaped curves are formed.

In the design process of the *S-shaped* droop curve, the curve must meet the requirement that the absolute value of $\mathrm{d}f/\mathrm{d}P$ at the point N is less than the absolute value of the linear droop curve (curve 1). In the position close to the microsource output power limits (0 and $P_{\max}$) the absolute value of the frequency speed ratio $\mathrm{d}f/\mathrm{d}P$ in the designed curve must be greater than the absolute value of $\mathrm{d}f/\mathrm{d}P$ in the linear droop curve to meet the consistent requirements of the proposed boundary curve design.

The $\mathrm{d}f/\mathrm{d}P$ curves $1'$, $2'$, $3'$, and $4'$ in the right part of Fig. 3 correspond to the curves 1, 2, 3, and 4 in the upper part of Fig. 3, respectively, k_{f10}, k'_{f20}, k'_{f30}, and k'_{f40} correspond to the $\mathrm{d}f/\mathrm{d}P$ values in the set of curves at the boundary and $|k_{f10}| < |k'_{f40}| < |k'_{f30}| < |k'_{f20}|$ indicates that the sensitivity of the frequency variation near the boundaries of the power output grows in the order of $1'$-$4'$-$3'$-$2'$. In the vicinity of the nominal point N, the sensitivity of the frequency variation gradually decreases in the order of $1'$-$4'$-$3'$-$2'$. In the case of the same size of output power, the frequency deviation range near the point N of the system in curve 2 is the lowest and the range in curve 1 is the highest and, vice versa for the deviation range near the boundaries. The actual $\mathrm{d}f/\mathrm{d}P$ value set needs to consider the combination of multiple inverters and the sensitivity of the frequency variation at the nominal point and the boundary points.

The aim of the proposed S-shaped droop design in inverter control is to have more share of load with less frequency deviation near the nominal point and less share of load around the boundary which is anticipated to protect the lifetime of the inverter. Therefore, the slope's absolute values should be lower near the nominal point and higher near the boundary points. In Fig. 3, the coefficient value near nominal point in curve 4 is set relatively greater than the corresponding value in the other design curves, which make the stability of power sharing better; the coefficient value near the upper limits is set relatively lower than the other curves, making it capable of more percentage output power than the other design curves. Thus, curve 4 is better than the other curves. As we can observe from Fig. 3, the S-shaped droop curve is symmetrical around the nominal operating point N, resulting in the $\mathrm{d}f/\mathrm{d}P$ value near the minimum boundary being approximately equal to the corresponding value near the maximum boundary in the right part of Fig. 3. The symmetry of the nominal operating point N in the S-shaped droop curve and the $\mathrm{d}f/\mathrm{d}P$ curve is affected by the position of the nominal operating point, the upper boundary limit, and the lower boundary limit. An asymmetrical S-shaped droop curve is shown in Fig. 4. This is due to the point N not being in the middle of the range $[0, P_{\max}]$.

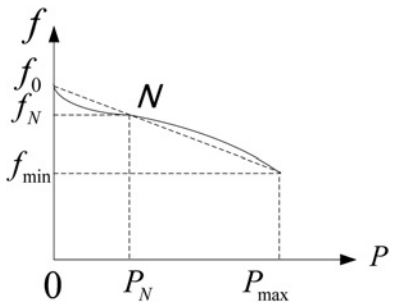

Fig. 4 *Asymmetric S-shaped P–f droop curve*

3.3 Modelling of S-shaped droop curve

As seen from the S-shaped droop curve in Fig. 3, if $P < P_N$, the curve segment opens upward and is located below the linear droop curve. If $P > P_N$, the curve segment opens downward and is located above the linear droop curve. Two curves are connected at the nominal operating point (rated power P_N and rated frequency f_N), where the first derivative exists. This ensures a smooth transition at the nominal point. According to the above design principle of the curve, the S-shaped droop characteristics can be theoretically achieved and the power output with a variable speed ratio can be realised according to different frequency offset ranges.

Many different forms of the mathematical model can be used to meet the above requirements in an S-shaped droop curve. Here, two typical models are presented as follows.

3.3.1 Third-order polynomial model: According to the characteristics of Fig. 3, the S-shaped droop curve can be described with a polynomial function, i.e. a third-order polynomial function, as shown in (1) and the df/dP function can be expressed as a quadratic polynomial function, as shown in (2)

$$f = a_f P^3 + b_f P^2 + c_f P + d_f \tag{1}$$

$$\mathrm{d}f/\mathrm{d}P = 3a_f P^2 + 2b_f P + c_f \tag{2}$$

Here, the frequency is a function of the output power P. Based on the power output limit setting (f_0 at the lower power limit 0 and $f_{\min}$ at the upper power limit $P_{\max}$), the nominal operation point parameters setting (P_N and f_N) and the frequency speed ratio setting (the df/dP value at the point N), the polynomial coefficients a_f, b_f, c_f, and d_f can be calculated. Thus, an accurate mathematical model for the S curve can be built.

3.3.2 Other possible mathematical model: The S-shaped droop curve can also be expressed in other mathematical models, such as the two piecewise quadratic polynomial function model with the df/dP curve described as a piecewise linear function (Fig. 5) or the multiple piecewise linear function model with the df/dP curve described as a piecewise step function (Fig. 6).

In the following analysis, the mathematical model is analysed using a third order polynomial function as the mathematical model

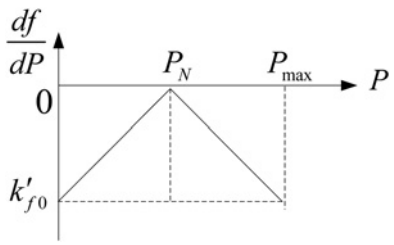

Fig. 5 *Piecewise linear df/dP curve*

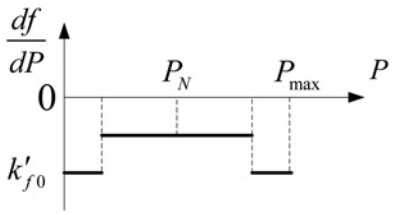

Fig. 6 *Piecewise step df/dP curve*

for simplicity. Similar works can be performed with other S-shaped models.

4 Analysis of S-shaped droop in *P–f* control among multi-inverters

Two inverters respectively controlled by the S-shaped droop and linear droop characteristic, namely hybrid control, will be analysed for compatibility and load sharing. Here, the self-regulation effect between load and frequency, namely the load increase with the frequency rising and the load decrease with the frequency being reduced, is considered.

In a test system consisting of two inverter-based sources, the case with hybrid control is defined as the *hybrid* case and the case with linear droop defined as the *contrast* case. The relationship between the active power and system frequency is conducted in (3) and (4), which describe the dynamics characteristics of the sources and the loads, in the hybrid case and the contrast case, respectively,

$$\Delta P_{\mathrm{L0}} = \Delta f_{\mathrm{s}}/k'_{f1} + \Delta f_{\mathrm{s}}/k_{f2} - K_L \cdot \Delta f_{\mathrm{s}} \tag{3}$$

$$\Delta P_{\mathrm{L0}} = \Delta f/k_{f1} + \Delta f/k_{f2} - K_{\mathrm{L}} \cdot \Delta f \tag{4}$$

where $k_{fi}(i = 1, 2)$ denotes the generator regulation coefficient (corresponding to the droop coefficient of inverter in linear droop) with a negative sign; k'_{f1} denotes the generator regulation coefficient in the S-shaped droop control with a negative sign; the static frequency adjustment effect coefficient of load is positive and is denoted by K_L; ΔP_{L0} denotes the load change quantity; and Δf and Δf_{s} are the frequency deviations by linear droop control and the S-shaped control, respectively. The respective sign of all variable, such as ΔP_{L0}, Δf, Δf_{s}, is defined as positive when the corresponding load power P_{L0} or the frequency f or f_{s} increases, and vice versa.

The analysis is carried out in the case of an increasing load. Since here the load increment in the above two cases is defined as identical ΔP_{L0} value, thus (3) and (4) are equal to each other and then (5) and (6) will be deducted. The left side of (5) demonstrates the inverter power output difference between the case with the S-shaped droop and linear droop control, namely, the difference between ΔP_{2s} and ΔP_2. If the difference is positive or negative, it means that the output power provided by the inverter with the S-shaped droop is more or less than the power by inverter with linear droop

$$(\Delta f_{\mathrm{s}}/k'_{f1}) - (\Delta f/k_{f1}) = (-1/k_{f2} + K_{\mathrm{L}}) \cdot (\Delta f_{\mathrm{s}} - \Delta f) \tag{5}$$

Defining $\Delta P_{2s} = \Delta f_{\mathrm{s}}/k'_{f1}$, $\Delta P_2 = \Delta f/k_{f1}$, we have

$$\Delta P_{2s} - \Delta P_2 = (-1/k_{f2} + K_{\mathrm{L}}) \cdot (\Delta f_{\mathrm{s}} - \Delta f) \tag{6}$$

4.1 Operation near the nominal point

Due to the droop coefficient absolute value near the nominal point in an S-shaped droop control is less than the corresponding value in a linear droop control, $\Delta f_{\mathrm{s}} > \Delta f$, namely $|\Delta f_{\mathrm{s}}| < |\Delta f|$, then we have $\Delta P_{2s} > \Delta P_2$. The conclusion is consistent with the practical condition that the output power from the inverter by the S-shaped control in the

hybrid case is greater than the power from the corresponding inverter in the contrast case. Meanwhile, the decreasing quantity due to load self-regulation by frequency droop is less than the corresponding quantity in the linear droop control. The hybrid case meets the load demand better than the contrast case.

4.2 Operation near the output power limits

The best way to protect the storage unit with limited energy is to operate it away from the power output limits. When the power value is close to the upper or lower limits, some measures should be taken to change the droop coefficient absolute value such that its load share is less than the other load share. For example, if it is close to the upper limits, $|k'_{f1}| > |k_{f2}|$ is set and $\Delta P_{2s} < \Delta P_2$ (i.e. the output power from the inverter controlled by the S-shaped droop is less than the power from the corresponding inverter in linear control). This result, with the appropriate frequency offset, can protect these inverter-based sources.

5 Analysis of S-shaped droop in *Q–U* control among multi-inverters

In practice, it is feasible for inverters to generate or absorb reactive power in order to maintain voltage stability and smooth reactive power compensation. The reactive power output control strategy of a power inverter is usually linear droop control, as shown in Fig. 3, where the droop characteristic is similar in the Q–U and P–f curves. The difference between the Q–U droop and P–f droop curves is as follows: (i) the reactive power output at zero corresponds to the rated voltage U_N; and (ii) the output reactive power can be positive or negative.

Similar to the S-shaped P–f droop curve design principles, the design of an S-shaped Q–U curve still needs to meet the upper and lower limits ($Q_{\max}$, $Q_{\min}$) of reactive power and rated operation point (U_N) conditions.

In the next simulation runs, the reactive and active power outputs are set to maintain the apparent power constant, so the reactive power will change in accordance with the active power output variation. In practical engineering projects concerning the distributed generations, usually, the active power control is the first factor to consider, so the aforementioned reactive power strategy is feasible. Also, the shortage of reactive power can be solved by means of the compensation device at the port of the inverter, or at other place using conventional devices like static capacitor banks.

6 Implementation of S-shaped droop characteristic in inverter control

Fig. 7 shows a schematic diagram of the DR unit, in a similar setting to [9]. The power circuit of the microsource unit consists of a conditioned prime energy source, a current-controlled voltage-sourced converter (VSC), and a three-phase filter. A three-phase LC filter is mounted at the port of every inverter. The per-phase resistance, inductance, and capacitance of the filter are denoted by R, L, and C, respectively. The resistance represents the ohmic loss of the filter inductor and also includes the effect of the on-state resistance of the VSC valves.

In general, a classic linear droop control structure is comprised of a power controller and current/voltage double control loops. The power controller consists of three parts: power calculation module, droop control module, and voltage synthesis module. The specific internal structure of each module is shown in Fig. 8. The power calculation module collects the load voltage and current via sensors to calculate the DG instantaneous power output and then obtain the average power P and Q via a low-pass filter, which is achieved by Discrete Mean Value models in Simulink/simpower system. According to the output P and Q, the frequency and output voltage amplitude, i.e. f and U, will be obtained by the droop control, where DG active power P and reactive power Q

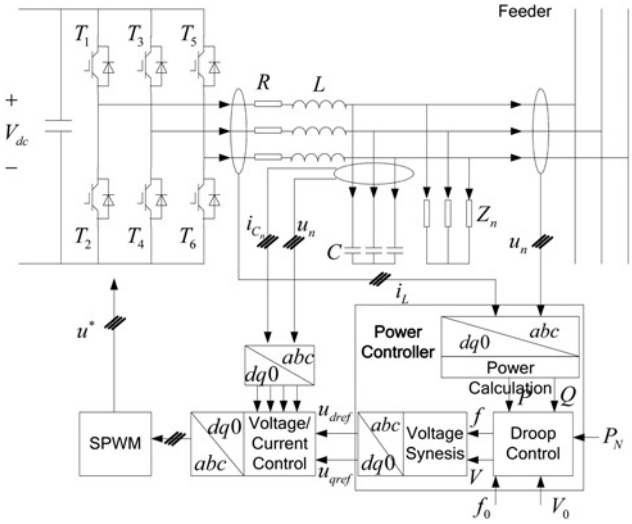

Fig. 7 *Inverter controller diagram*

must meet the two conditions: $0 \le P \le P_{\max}$ and $Q_{\min} \le Q \le Q_{\max}$. The voltage synthesis controller uses frequency f and voltage U to generate a three-phase symmetrical voltage reference u_{ref}, and obtain $u_{d\text{ref}}$ and $u_{q\text{ref}}$ by dq transformation, which acts as the input voltage and current to the double loop controller. The output is the controllable sinusoidal modulation signal u, which is input into the sinusoidal pulse-width modulation module.

The proposed S-shaped droop curve inherits the characteristics of an automatic share of the load from synchronous generators and retains the 'plug and play' ability of a linear droop control inverter. The only difference between the S-shaped curve and the linear curve is that the slope of the S-shaped curve is not constant, but variable. The third-order polynomial function in (1) in Section 3 will be used to design an S-shaped droop curve.

The slope k'_f of an S-shaped droop curve in the P–f plane is given as follows

$$k'_f = \mathrm{d}f/\mathrm{d}P = 3a_f P^2 + 2b_f P + c_f \tag{7}$$

The slope k'_u of an S-shaped droop curve in Q–U plane is given as follows

$$k'_u = \mathrm{d}U/\mathrm{d}Q = 3a_u Q^2 + 2b_u Q + c_u \tag{8}$$

In Fig. 7, the slopes k_f and k_u are, respectively, replaced by k'_f and k'_u, and then the implementation of the S-shaped droop control block can be carried out.

7 Simulation and analysis

In order to verify the feasibility of the S-shaped droop applied in the microgrid inverter control, a simulation study is carried out in Matlab/Simulink. The test microgrid circuit is powered by two inverter

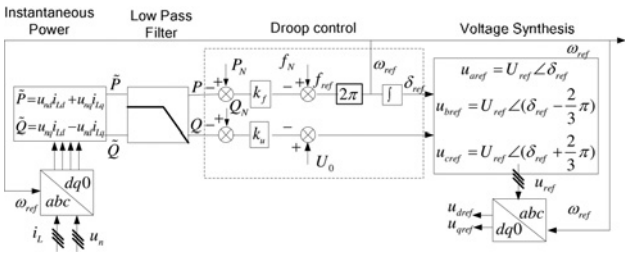

Fig. 8 *Power controller diagram*

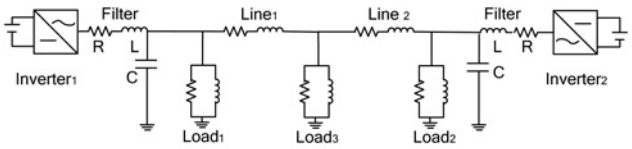

Fig. 9 *Microgrid powered by two inverters diagram*

Table 1 Simulation parameters of test system

Sources	$U_{dc} = 800$ V, $P_N = 50$ kW, $f_N = 50$ Hz, $U_N = 380$ V; Frequency = 50 Hz
Filter	$R = 0.01\ \Omega$; $L = 6 \times 10^{-4}$ H; $C = 1.5 \times 10^{-3}$ F
Carrier frequency	6000 Hz (discrete three-phase pulse-width modulation generator)
Line	$Z_{line1} = Z_{line2} = 0.06 + j0.1885\ \Omega$;
S-shaped control	$k'_f = -2.4 \times 10^{-15} \times P^2 + 2.4 \times 10^{-10} \times P - 1.2 \times 10^{-5}$ $k'_u = -2 \times 10^{-13} \times Q^2 - 1 \times 10^{-4}$
Linear control	$k_f = -1 \times 10^{-5}$; $k_u = -3 \times 10^{-4}$
Normal range	$Load_1 = Load_2 = 40 + j20$ kVA; $Load_3 = 60 + j30$ kVA
Output limits	$Load_1 = Load_2 = 50 + j25$ kVA; $Load_3 = 100 + j50$ kVA

sources with identical parameters, as shown in Fig. 9. To compare the control effect between the S-shaped droop control and the conventional linear droop control, the studies are divided into two cases: a *hybrid* case and a *contrast* case. In the hybrid case with the subscripts 1 or 2, one inverter is under S-shaped control, denoted as '*non-linear*', and the other one is under linear control, denoted as '*linear*'. In the contrast case, both inverters are controlled by the identical linear control with the subscripts 3 or 4. After the test, the output active and reactive powers will be compared to demonstrate the difference between the aforementioned control methods. Finally, the anti-disturbance ability of the system will be analysed to observe the stability to sudden load variations.

The simulation setup is described next. The total duration of the simulation is 1 s; the sampling interval is 5×10^{-5} s. The physical parameters of the two inverters are identical. The common load parameters powered by the two micro-sources are different in following tests. There are only two sets of control parameters for the inverters to select and these are described in Table 1.

7.1 Load sharing test

7.1.1 Operation in the normal range: This test is to confirm load sharing effects between different control technologies in the normal range, and the test result is demonstrated in Fig. 10, in which the active power, reactive power, and frequency variation curves in these two cases are demonstrated. In Fig. 10*a*, the *black-solid* and *grey-solid* curves, denoted by *P1-non-linear* and *Q1-non-linear*, are the active and reactive power respectively by the S-shaped control method; while the black-dashed and grey-dashed curves denote the output of the linearly controlled inverter, denoted by *P2-linear* and *Q2-linear*.

In the contrast case controlled by the linear droop in Fig. 10*b*, two inverters can share the load evenly, as shown by *P3-linear* (P3 output in the contrast case) and *P4-linear* (P4 output in the contrast case), which are reasonably close. However, the non-linear control method in one inverter results the difference observed. As seen from Fig. 10*a*, *P1-non-linear* is considerably higher than *P2-linear*.

This confirms the first expectation implied in (6) in Section 4. That is, with the S-shaped droop control, the output near the nominal point is more than that of linear droop.

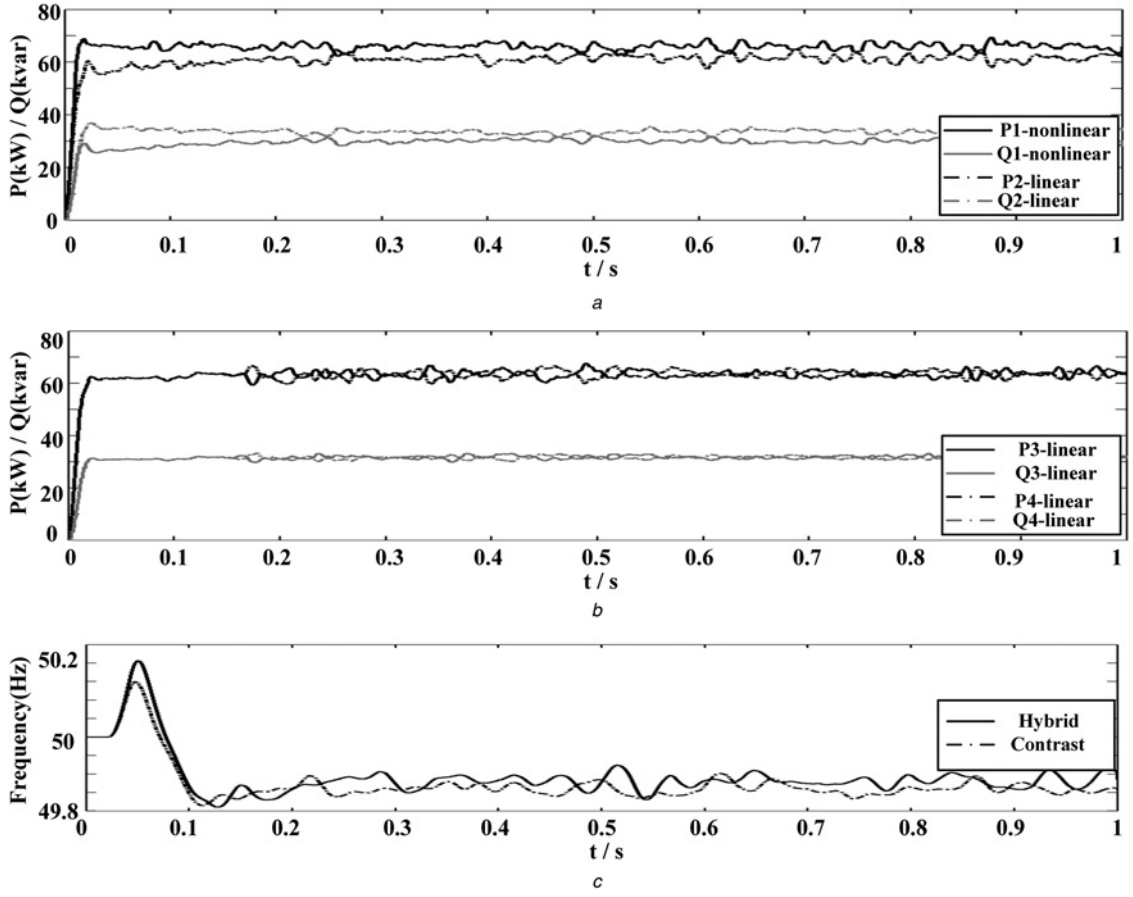

Fig. 10 *Inverter output in the normal range*

a Power sharing result between the nonlinear and linear control inverters in hybrid case
b Power sharing result between the identical linear control inverters in contrast case
c Frequency variation

Table 2 Comparison under normal range

	P_1, kW	Q_1, kvar	P_2, kW	Q_2, kvar	f, Hz
contrast case	64.01	31.72	63.76	32.03	49.86
hybrid case	66.39	31.01	61.97	33.04	49.89
total load			140 + 70 kVA		

Table 3 Comparison for the studies near output power limits

	P_1, kW	Q_1, kvar	P_2, kW	Q_2, kvar	f, Hz
contrast case	86.87	42.66	86.19	43.33	49.65
hybrid case	83.65	44.43	88.36	41.00	49.74
total load			200 + j100 kVA		

As can be seen in Fig. 10*c*, the frequency variation is stable after the former period, approximate 0.02 s, and the swing magnitude of the curve is low. Therefore, the nonlinearity has little effect on frequency stability.

The data is extracted from Fig. 10 in the last five cycles, which last 0.1 s. The data concerning the active power, the reactive power, and the frequency are all shown in Table 2.

From Table 2, we can observe that with the same load demand in a normal range, the 0.11 Hz deviation of the *frequency-hybrid* in the hybrid case is less than the 0.14 Hz deviation of the *frequency-contrast* in the contrast case. At the same time, the total active power output of the hybrid case is 0.59 kW greater than that of the contrast case, namely, a lower load reduction due to the frequency drop in the hybrid case. Thus, it can be concluded that the S-shaped control demonstrates a partial secondary frequency control (i.e. speed-changer setting), since the power output in the hybrid case is more than that from the contrast case of linear droop.

7.1.2 Operation near the output power limits: The purpose of this test is to demonstrate the load sharing effect between different control technologies when the system operating point is close to the output limits. In Fig. 11, the lower black-solid curve *P1-non-linear* and the upper black-dash curve *P2-linear* in the active power curves of Fig. 11*a* illustrate that the power output from the inverter by the S-shaped droop is less than that from the inverter by the linear droop near the output limits. Meanwhile, *P3-linear* and *P4-linear* are much closer to each other, which shows linear droop tends to give equal shares of the load change among two generators.

The data is extracted from Fig. 11 in the last five cycles and the extracting method is the same as in the previous test. The extracted data is described in Table 3.

With limited improvement of frequency deviations (from 49.65 to 49.74 Hz), the 83.65 kW output of the first inverter with the S-shaped droop control is less than the 86.87 kW output of the same inverter with the linear droop control in the contrast case. The output of the second inverter under linear droop control increases from 86.19 kW from the contrast case to 88.36 kW in the hybrid case. With the total load demand being met, part of the load sharing is transferred to other sources with certain reserve capacity. The above data demonstrates the realisation of a control

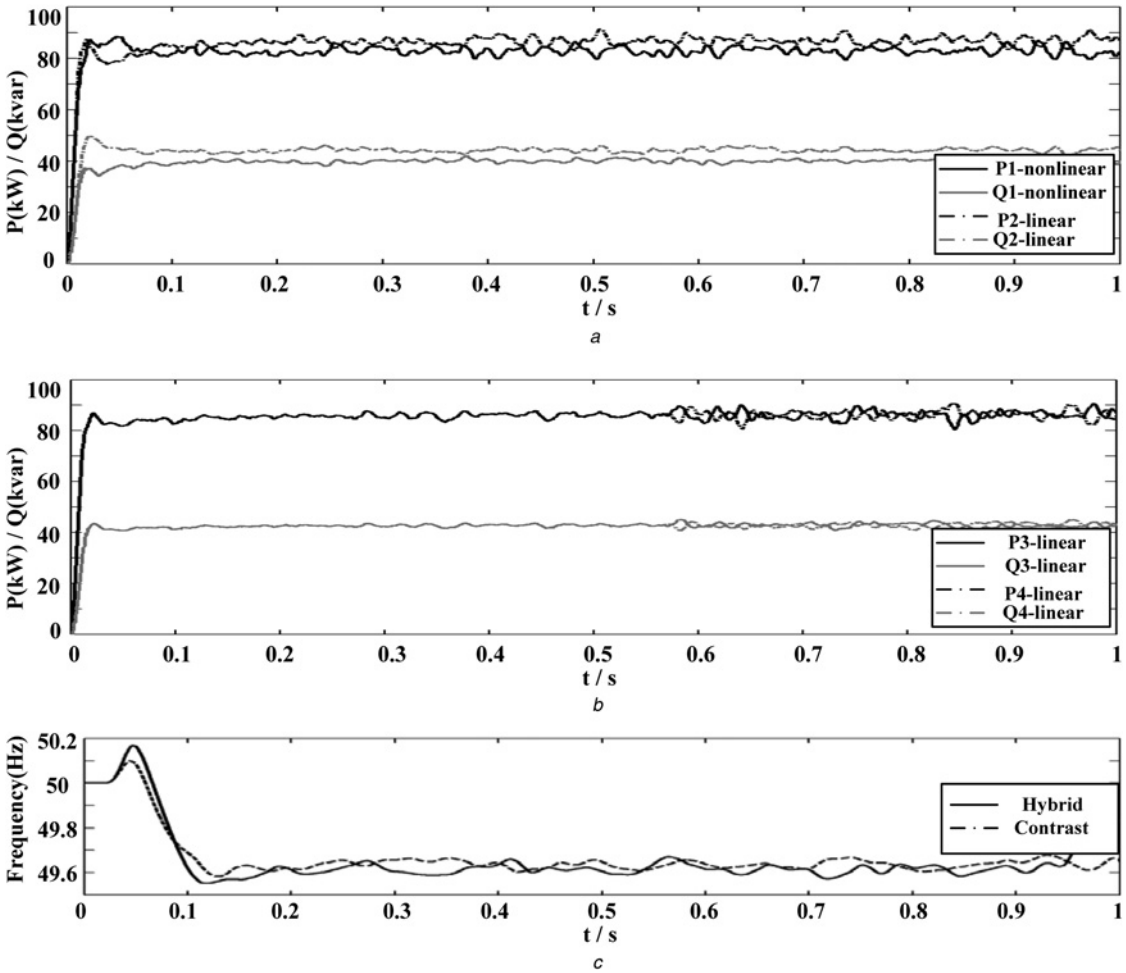

Fig. 11 *Inverter output near the power limits*

a Power sharing result between the nonlinear and linear control inverters in hybrid case
b Power sharing result between the identical linear control inverters in contrast case
c Frequency variation

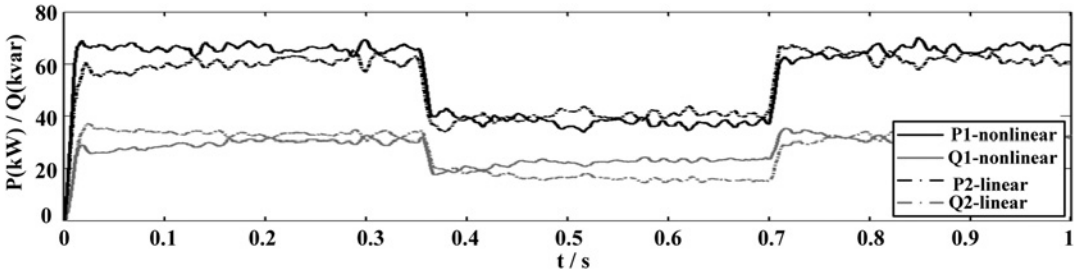

Fig. 12 *Test simulation of anti-disturbance*

strategy with load transfer, output reduction, and source protection in the inverter by the S-shaped droop.

With the same load demand, the hybrid control strategy causes the voltage frequency deviation (0.26 Hz) to be lower than the deviation in the contrast case (0.35 Hz). To a certain extent, the frequency quality is improved and a secondary frequency control effect is somewhat reflected in the S-shaped control since the frequency is higher in the hybrid case.

7.1.3 Discussion about the output reactive power: As seen in the hybrid case in Figs. 10, 11 and Tables 2, 3, the output power comparison between the inverters controlled by the *S-shaped* droop and by the linear droop is demonstrated. In Fig. 10, the *P1-non-linear* value is more than the *P2-linear* value, and *Q1- non-linear* value is less than *Q2-linear* value. In Fig. 11, the opposite to Fig. 10 can be observed. The reason is analysed as follows.

Due to the control module in Section 6, the reference of the inverter output voltage magnitude is adjusted according to the feedback value of the load terminal voltage. The feedback relation results in that inverter output voltage magnitude changes with the voltage drop due to line impedance and transmission power. The more the inverter output apparent power, the more the line voltage drop, the less of the inverter voltage is achieved. The lower voltage magnitude will result in less reactive power. From the previous figures and tables, the active power percentage is more than the reactive power percentage in the apparent power. Therefore, the active power is the leading factor that affects the voltage magnitude. As a result, in the comparison between the hybrid and contrast cases, the *P1-non-linear* value is more than *P2-linear*, and then the *Q1-non-linear* value is less than *Q2-linear*, and vice versa.

7.2 Anti-disturbance analysis

Here, the disturbance is set up for testing the hybrid control in which load 3 is disconnected at $t = 0.35$ s and re-connects at $t = 0.70$ s. The load parameters are the same as in the test in Section 7.1.1.

As seen in Fig. 12, the fluctuations of active power, reactive power, and frequency are all small and a smooth transition is maintained during the disconnection or re-connection of the load 3. The transition time is short (maximum is 0.011 s); the maximum oscillation amplitudes of active and reactive powers are, respectively, ±5 kW and ±3 kvar, which is perfectly acceptable for the 140 kW and 70 kvar load. The transition of the frequency is smooth, with a 0.075 s transition time when load 3 is disconnected at 0.35 s and with a 0.1 s transition time when load 3 is re-connected at 0.7 s. The maximum oscillation amplitude is ±0.05 Hz. A longer transition time essentially ensures a smooth and stable frequency transition.

8 Conclusions

In this paper, the frequency deviation problems in traditional linear droop control are improved by means of an S-shaped droop control strategy, which fits the output characteristics of the inverter power. On one hand, when the system is operated at around the nominal operation point (i.e. rated frequency and rated voltage), load fluctuations will be met by the inverter source output as soon as possible with the frequency fluctuation being as small as possible. On the other hand, when the output power is close to the upper or lower limits of a certain microsource's capacity, the share of total load demand to this microsource should be smaller than the share from the other sources, which will achieve a complementary effect among microsources with different power capacities.

9 Acknowledgment

J. Li and F. Li acknowledge the support provided by CURENT, an Engineering Research Center (ERC) Program of NSF and DOE under NSF grant EEC-1041877. Also, J. Li, X. Li, H. Liu, F. Chen and B. Liu acknowledge the support in part from the Project on the Integration of Industry, Education and Research of Jiangsu Province (BY2015009-03), the Foundation of Nanjing Institute of Technology (ZKJ201304, CKJA201406), the Brand Professional Construction Project of Jiangsu Province (PPZY2015A031), and the National Natural Science Foundation of China (Grant No. 51577086).

10 References

1 Mohda, A., Ortjohanna, E., Mortonb, D., *et al.*: 'Review of control techniques for inverters parallel operationz', *Electr. Power Syst. Res.* , 2010, **80**, pp. 1477–1487
2 Guerrero, J., Vasquez, J., Matas, J., *et al.*: 'Control strategy for flexible microgrid based on parallel line-interactive UPS systems', *IEEE Trans. Ind. Electron.*, 2009, **56**, (3), pp. 726–736
3 Iyer, S.V., Belur, M.N., Chandorkar, M.C.: 'A generalized computational method to determine stability of a multi-inverter microgrid', *IEEE Trans. Power Electron.*, 2010, **25**, (9), pp. 2420–2432
4 Majumder, R., Chaudhuri, B., Ghosh, A., *et al.*: 'Improvement of stability and load sharing in an autonomous microgrid using supplementary droop control loop', *IEEE Trans. Power Syst.*, 2010, **25**, (2), pp. 796–808
5 Chandorkar, M., Divan, D., Adapa, R.: 'Control of parallel connected inverters in standalone AC supply systems', *IEEE Trans. Ind. Appl.*, 1993, **29**, (1), pp. 136–143
6 Guerrero, J.M., Vásquez, J.C., Matas, J., *et al.*: 'Hierarchical control of droop-controlled AC and DC microgrids – a general approach toward standardization', *IEEE Trans. Ind. Electron.*, 2011, **58**, (1), pp. 158–172
7 De Brabandere, K., Bolsens, B., Van den Keybus, J., *et al.*: 'A voltage and frequency droop control method for parallel inverters', *IEEE Trans. Power Electr.*, 2007, **22**, (4), pp. 1107–1115
8 Katiraei, F., Iravani, M.R., Lehn, P.W.: 'Microgrid autonomous operation during and subsequent to islanding process', *IEEE Trans. Power Deliv.*, 2005, **20**, (1), pp. 248–257
9 Delghavi, M.B., Yazdani, A.: 'An adaptive feedforward compensation for stability enhancement in droop-controlled inverter-based microgrids', *IEEE Trans. Power Deliv.*, 2011, **26**, pp. 1764–1773
10 Quesada, J., Sebastián, R., Castro, M., *et al.*: 'Control of inverters in a low voltage microgrid with distributed battery energy storage, part I: primary control', *Electr. Power Syst. Res.* , 2014, **114**, pp. 126–135
11 Tian-Yong, G., Geng-Shen, Z., Yao, Z., *et al.*: 'Modeling and simulation of microgrid system based on wind-solar hybrid', *Power Syst. Prot. Control (in Chinese)*, 2010, **38**, pp. 104–106
12 Marwali, M., Jung, J.-W., Keyhani, A.: 'Control of distributed generation systems – Part II: Load sharing control', *IEEE Trans. Power Electron.*, 2004, **19**, (6), pp. 1551–1561
13 Zhong, Q.-C.: 'Robust droop controller for accurate proportional load sharing among inverters operated in parallel', *IEEE Trans. Ind. Electron.*, 2013, **60**, pp. 1281–1290
14 Simpson-Porco, J.W., Dörfler, F., Bullo, F.: 'Synchronization and power sharing for droop-controlled inverters in islanded microgrids', *Automatica*, 2013, **49**, pp. 2603–2611
15 Quesada, J., Sebastián, R., Castro, M., *et al.*: 'Control of inverters in a low voltage microgrid with distributed battery energy storage, part II: secondary control', *Electr. Power Syst. Res.* , 2014, **114**, pp. 136–145